WDR41 supports lysosomal response to changes in amino acid availability

Joseph Amick, Arun Kumar Tharkeshwar, Catherine Amaya, and Shawn M. Ferguson*
Department of Cell Biology and Program in Cellular Neuroscience, Neurodegeneration and Repair, Yale University School of Medicine, New Haven, CT 06510

ABSTRACT **C9orf72 mutations are a major cause of amyotrophic lateral sclerosis and frontotemporal dementia. The C9orf72 protein undergoes regulated recruitment to lysosomes and has been broadly implicated in control of lysosome homeostasis. However, although evidence strongly supports an important function for C9orf72 at lysosomes, little is known about the lysosome recruitment mechanism. In this study, we identify an essential role for WDR41, a prominent C9orf72 interacting protein, in C9orf72 lysosome recruitment. Analysis of human WDR41 knockout cells revealed that WDR41 is required for localization of the protein complex containing C9orf72 and SMCR8 to lysosomes. Such lysosome localization increases in response to amino acid starvation but is not dependent on either mTORC1 inhibition or autophagy induction. Furthermore, WDR41 itself exhibits a parallel pattern of regulated association with lysosomes. This WDR41-dependent recruitment of C9orf72 to lysosomes is critical for the ability of lysosomes to support mTORC1 signaling as constitutive targeting of C9orf72 to lysosomes relieves the requirement for WDR41 in mTORC1 activation. Collectively, this study reveals an essential role for WDR41 in supporting the regulated binding of C9orf72 to lysosomes and solidifies the requirement for a larger C9orf72 containing protein complex in coordinating lysosomal responses to changes in amino acid availability.**

Monitoring Editor
Francis A. Barr
University of Oxford

Received: Dec 7, 2017
Revised: Jun 22, 2018
Accepted: Jul 2, 2018

INTRODUCTION

Expansions of a hexonucleotide repeat within a noncoding region of the C9orf72 gene are a major cause of amyotrophic lateral sclerosis (ALS) and frontotemporal dementia (FTD) (DeJesus-Hernandez *et al.*, 2011; Renton *et al.*, 2011; Gijselinck *et al.*, 2012). Multiple mechanisms have been proposed to explain how these C9orf72 mutations cause neurodegenerative disease. One possible contributing factor is C9orf72 protein haploinsufficiency as the hexanucleotide repeat expansions are accompanied by a reduction in C9orf72 mRNA and protein levels (DeJesus-Hernandez *et al.*, 2011; Gijselinck *et al.*, 2012; Belzil *et al.*, 2013; van Blitterswijk *et al.*, 2015; Amick and Ferguson, 2017; Shi *et al.*, 2018). The potential disease implications of reduced C9orf72 expression have motivated efforts to elucidate the direct cellular functions of the C9orf72 protein. From a cell biology perspective, we previously discovered that C9orf72 is recruited to lysosomes in response to amino acid deprivation (Amick *et al.*, 2016). The physiological relevance of C9orf72 lysosome localization is supported by multiple lysosome defects that have been observed in mammalian C9orf72 knockouts (Amick *et al.*, 2016; O'Rourke *et al.*, 2016; Sullivan *et al.*, 2016; Ugolino *et al.*, 2016). Most recently, functions in the endo-lysosomal pathway were also established for the *Caenorhabditis elegans* C9orf72 ortholog (Corrionero and Horvitz, 2018). The evolutionarily conservation of a role for C9orf72 in the regulation of lysosome homeostasis combined with human C9orf72 mutations as a cause of neurodegenerative disease indicates that elucidation of C9orf72 functions and regulatory mechanisms has broad cell biological relevance with the added potential of shedding light on neurodegenerative disease pathogenesis.

An important insight into potential functions for the C9orf72 protein came from bioinformatic analyses that predicted that it contains

This article was published online ahead of print in MBoC in Press (http://www.molbiolcell.org/cgi/doi/10.1091/mbc.E17-12-0703) on July 11, 2018.
The authors declare no competing financial interests.
*Address correspondence to: Shawn M. Ferguson (shawn.ferguson@yale.edu).
Abbreviations used: ALS, amyotrophic lateral sclerosis; C9orf72, chromosome 9 open reading frame 72; CRISPR, clustered regularly interspaced short palindromic repeats; DAPI, 4′,6-diamidino-2-phenylindole; DENN, differentially expressed in normal and neoplastic cells; EGTA, egtazic acid; FLCN, folliculin; FNIP, FLCN-interacting protein; FTD, frontotemporal dementia; GAP, GTPase-activating protein; GEF, guanine nucleotide exchange factor; GFP, green fluorescent protein; HA, hemagglutinin; IP, immunoprecipitation; KO, knockout; LAMP1, lysosome-associated membrane protein 1; LC3, microtubule-associated proteins 1A/1B light chain 3; mTORC1, mechanistic target of rapamycin complex 1; PBS, phosphate-buffered saline; RB1CC1, RB1-inducible coiled-coil 1; sgRNA, single-guide RNA; SMCR8, Smith-Magenis Chromosome Region gene 8; ULK, Unc-51-like kinase; WDR41, WD repeat-containing protein 41; WT, wild type.

a differentially expressed in normal and neoplastic cells (DENN) domain and is most similar to a branch of the DENN domain family containing folliculin (FLCN), FLCN-interacting proteins (FNIPs), and the Smith-Magenis Chromosome Region 8 (SMCR8) protein (Zhang *et al.*, 2012; Levine *et al.*, 2013). Subsequent studies revealed a strong physical interaction between C9orf72 and SMCR8 (Amick *et al.*, 2016; Sellier *et al.*, 2016; Sullivan *et al.*, 2016; Ugolino *et al.*, 2016; Xiao *et al.*, 2016; Yang *et al.*, 2016; Jung *et al.*, 2017) that parallels the interaction between FLCN and FNIPs (Baba *et al.*, 2006; Hasumi *et al.*, 2008; Takagi *et al.*, 2008; Amick and Ferguson, 2017). Interestingly, both the FLCN-FNIP and C9orf72-SMCR8 complexes localize to lysosomes (Petit *et al.*, 2013; Amick *et al.*, 2016). The FLCN–FNIP complex interacts with the lysosome-localized Rag GTPases (Petit *et al.*, 2013; Meng and Ferguson, 2018) and promotes mTORC1 signaling when amino acids are abundant by acting as a GTPase-activating protein (GAP) for RagC/D (Tsun *et al.*, 2013; Peli-Gulli *et al.*, 2015). While it is reasonable to speculate that the FLCN–FNIP and C9orf72–SMCR8 complexes may have similar functions at lysosomes, understanding of C9orf72 and SMCR8 functions and regulatory mechanisms remains more limited.

WDR41 was recently identified as a high-stoichiometry C9orf72–SMCR8 interacting protein through proteomic analyses of anti-C9orf72 immunoprecipitates (Sellier *et al.*, 2016; Sullivan *et al.*, 2016; Xiao *et al.*, 2016; Yang *et al.*, 2016). WDR41 belongs to a large family of WD-repeat-containing proteins that often function as scaffolds through their ability to interact with multiple proteins and/or lipids (Dove *et al.*, 2004; Jeffries *et al.*, 2004; Stirnimann *et al.*, 2010) and could thus play a role in regulating the stability and/or subcellular localization of C9orf72 and SMCR8. In contrast to the C9orf72–SMCR8–WDR41 complex, the better-understood FLCN–FNIP complex is not known to contain WDR41 or an equivalent WD-repeat-containing protein and thus does not provide clues concerning potential WDR41 functions. Thus, although the physical interaction between C9orf72 and WDR41 is well established, the functional relevance of this interaction and its relationship (if any) to C9orf72 functions at lysosomes was not previously determined.

In the present work, we show that WDR41 is required for the recruitment of C9orf72 and SMCR8 to lysosomes and that WDR41 itself localizes to lysosomes. This recruitment of the C9orf72–SMCR8–WDR41 complex to lysosomes occurs most prominently in starved cells but is independent of changes in mTORC1 or Unc-51-like kinase (ULK) complex signaling that occur under such conditions. Likewise, the association of the C9orf72–SMCR8–WDR41 complex with lysosomes does not depend on autophagy. Analysis of WDR41 knockout cells revealed a defect in the acute activation of mTORC1 by amino acids; this requirement for WDR41 could be bypassed by expression of a lysosome-targeted version of C9orf72. Taken together, our data indicate a major function of WDR41 is the recruitment of C9orf72 and SMCR8 to lysosomes.

RESULTS

WDR41 interacts with C9orf72

As a first step toward elucidating WDR41 function, we used CRISPR-Cas9 to generate WDR41 knockout (KO) cell lines (Supplemental Figure S1A). These efforts were successfully carried out in both HeLa cells as well as in a HEK293FT cell line that we previously engineered to express 2xhemagglutinin (HA) tagged-C9orf72 from its endogenous locus (Amick *et al.*, 2016). DNA sequencing (Supplemental Figure S1B) as well as anti-WDR41 immunoblots (Figure 1, A and B) confirmed that the WDR41 KO strategy was successful. Additional immunoblotting for C9orf72 and SMCR8 did not reveal changes in their levels following loss of WDR41 (Figure 1, A and B). This stands in contrast to the previously observed reciprocal dependence of C9orf72 and SMCR8 on one another for their stability (Amick *et al.*, 2016). In addition to the maintained stability of C9orf72 and SMCR8 in the absence of WDR41, the interaction between C9orf72 and SMCR8 was also not impaired in WDR41 KO cells (Figure 1C). The interaction of WDR41 is specific to the C9orf72 complex, as WDR41 did not coimmunoprecipitate with the structurally related FLCN–FNIP complex (Figure 1D). To gain further insight into interactions among WDR41, C9orf72, and SMCR8, C9orf72+SMCR8 double KO cells (Amick *et al.*, 2016) were transfected with GFP-tagged forms of C9orf72 or SMCR8 and subjected to anti-GFP immunoprecipitations. Although WDR41 copurified with GFP-C9orf72 in the absence of SMCR8 (Figure 1E), we did not detect a similar interaction between SMCR8-GFP and WDR41 in the absence of C9orf72. This selective interaction of C9orf72 with WDR41 in cells lacking SMCR8 supports a model wherein C9orf72 is the major determinant of WDR41 incorporation into this heterotrimeric protein complex (Figure 1F).

WDR41 is required for C9orf72 and SMCR8 recruitment to lysosomes

To investigate WDR41 function, we next used the WDR41 KO; 2xHA-C9orf72 HEK293FT cells to investigate the contribution of WDR41 to regulation of C9orf72 subcellular localization. We focused in particular on the localization of C9orf72 in starved cells, as we previously established that C9orf72 is recruited to lysosomes under such conditions (Amick *et al.*, 2016). The loss of lysosome-localized C9orf72 in WDR41 KO cells revealed that WDR41 is essential for the recruitment of C9orf72 to lysosomes (Figure 2, A and B). Transduction of WDR41 KO cells with a lentivirus encoding WDR41 rescued starvation triggered localization of C9orf72 to lysosomes, establishing the specificity of the WDR41 KO phenotype (Figure 2, A–C). Thus, while WDR41 is not critical for C9orf72 stability, it is essential for the regulated recruitment of C9orf72 to lysosomes when cells are deprived of amino acids. Although WDR41 is strikingly required for C9orf72 localization to lysosomes in starved cells, immunoprecipitation experiments revealed that the interaction among WDR41, C9orf72, and SMCR8 is constitutive and not changed in response to starvation (Supplemental Figure S1C).

As a complementary approach for testing the role for WDR41 in controlling both C9orf72 and SMCR8 abundance at lysosomes, we analyzed lysosomes that were purified from wild-type and WDR41 KO HeLa cells. To this end, lysosomes were magnetically isolated from cells that had been endocytically preloaded with iron dextran nanoparticles (Walker and Lloyd-Evans, 2015). This purification strategy resulted in the selective enrichment of lysosomal proteins by ~40 fold (Figure 3, A and B). We then measured the levels of C9orf72 and SMCR8 on lysosomes purified from wild-type and WDR41 KO cells under both fed and starved conditions. Although both C9orf72 and SMCR8 were robustly enriched on the lysosomes from starved wild-type cells, this effect was abolished in the WDR41 KO cells (Figure 3, C–E). Interestingly, there was also a low level of lysosomal C9orf72 and SMCR8 under fed conditions that was lost in the WDR41 KO cells (Figure 3, C–E). WDR41 is thus essential for recruitment of C9orf72 and SMCR8 to lysosomes. Evidence supporting the recruitment of SMCR8 to lysosomes is also noteworthy as this property was previously predicted (Amick *et al.*, 2016) but not directly demonstrated.

The discovery that WDR41 plays a critical role in the regulated recruitment of C9orf72 and SMCR8 to lysosomes raised questions concerning the specific mechanisms that allow WDR41 to perform such a function. The strong interaction between WDR41 and C9orf72 (Sellier *et al.*, 2016; Sullivan *et al.*, 2016; Ugolino *et al.*, 2016;

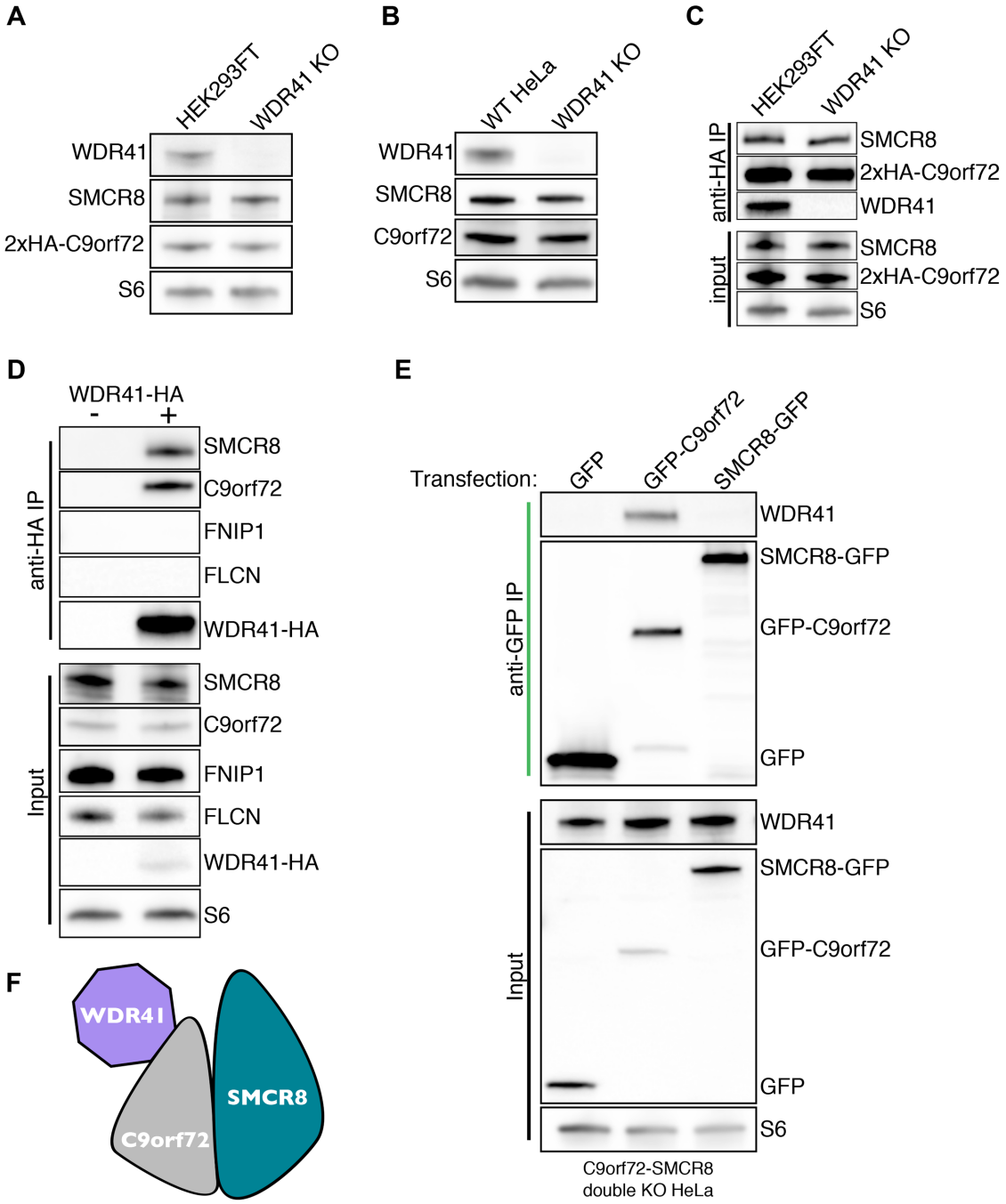

FIGURE 1: WDR41 interacts with C9orf72 but is not required for the stability of C9orf72 and SMCR8. (A) Immunoblot analysis of WDR41 KO in HEK293FT cells that express 2xHA-tagged C9orf72 from the endogenous locus. (B) Immunoblot analysis of control and WDR41 KO HeLa cells. (C) Endogenously expressed 2x-HA C9orf72 was immunoprecipitated from the parental and WDR41 knockout cell line, followed by immunoblotting for the indicated proteins. (D) Anti-HA immunoprecipitation of control and WDR41-HA-transfected HeLa cells followed by immunoblotting for the indicated proteins. (E) C9orf72/SMCR8 double knockout cells were transfected with GFP, GFP-C9orf72, or SMCR8-GFP followed by anti-GFP immunoprecipitation and immunoblotting for the indicated proteins. (F) Immunoprecipitation results in E support a model wherein WDR41 associates with the C9orf72:SMCR8 complex primarily via an interaction with C9orf72.

Xiao *et al.*, 2016; Yang *et al.*, 2016; Jung *et al.*, 2017) combined with the important role for WDR41 in supporting C9orf72 and SMCR8 localization to lysosomes suggested the presence of WDR41 itself at lysosomes. This prediction is supported by our observation that the interaction among WDR41, C9orf72, and SMCR8 is constitutive and not modulated by changes in amino acid availability (Supplemental Figure S1C). However, overexpressed GFP-tagged WDR41 was previously observed at the *cis*-Golgi rather than lysosomes (Sullivan *et al.*, 2016). Such a subcellular localization does not fit with a direct role for WDR41 in the recruitment of C9orf72 and SMCR8 to lysosomes and could reflect either an additional role for WDR41 at the Golgi or an artifact arising from the tagging and/or overexpression.

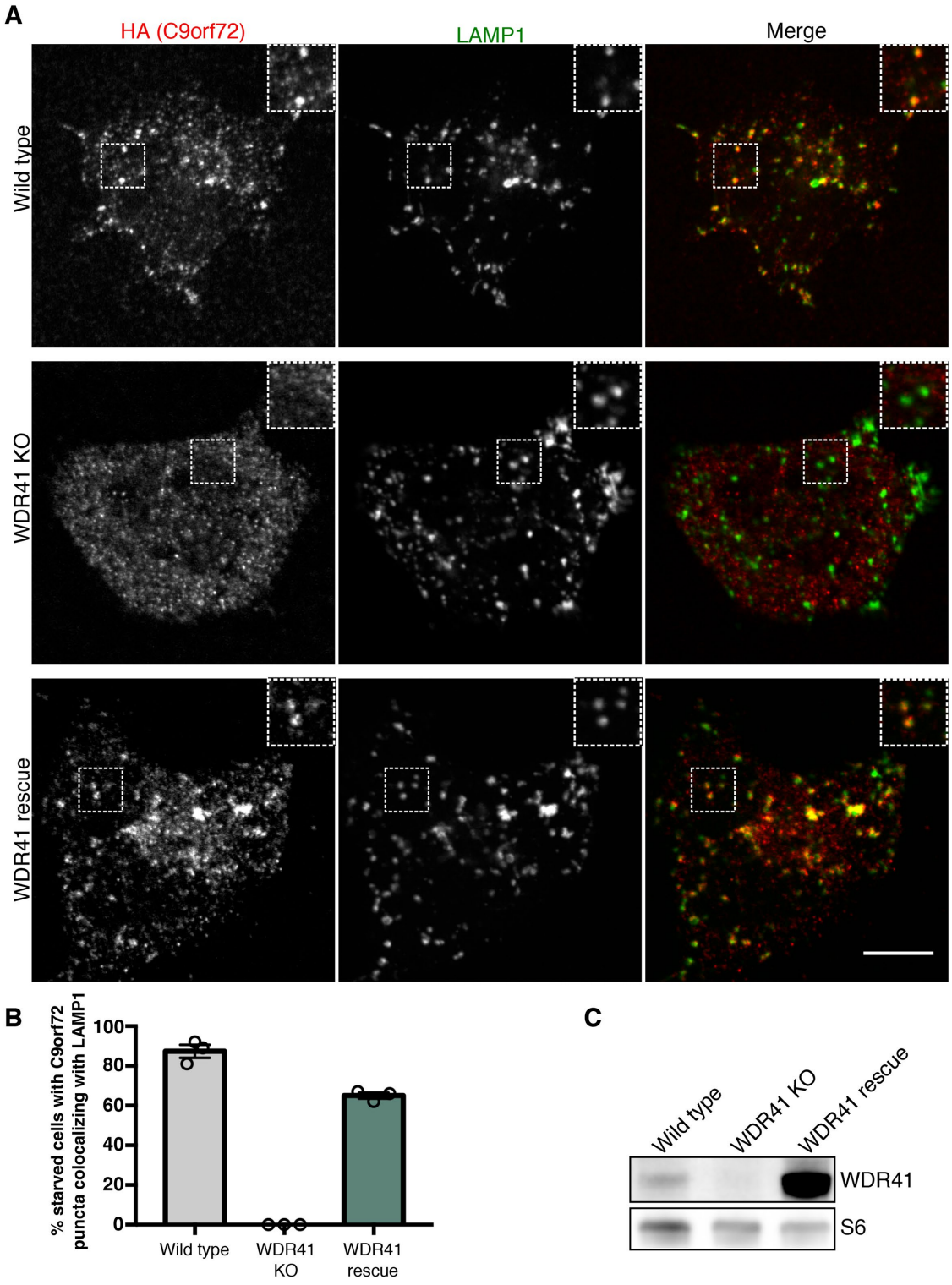

FIGURE 2: WDR41 is required for the recruitment of C9orf72 to lysosomes. (A) Immunofluorescence images of C9orf72 localization (endogenously expressed 2xHA-C9orf72) in starved wild-type, WDR41 knockout, and WDR41 KO cells that were rescued by stable expression of a WDR41 transgene. Localization of C9orf72 to lysosomes (LAMP1 signal) is lost in WDR41 knockout cells. Scale bar, 10 μm. (B) For the indicated cell lines, the percentage of cells in starved conditions containing C9orf72 puncta that colocalize with LAMP1 are indicated. (C) Immunoblot analysis of WDR41 levels in wild-type, knockout, and rescue cell lines.

WDR41 localizes to lysosomes

To directly visualize the subcellular localization of the endogenously expressed WDR41, we next sought to perform immunofluorescence experiments. Owing to the lack of validated WDR41 antibodies for immunofluorescence studies, we used CRISPR/Cas9-mediated genome editing to insert a 2xHA tag into the C-terminus of the WDR41

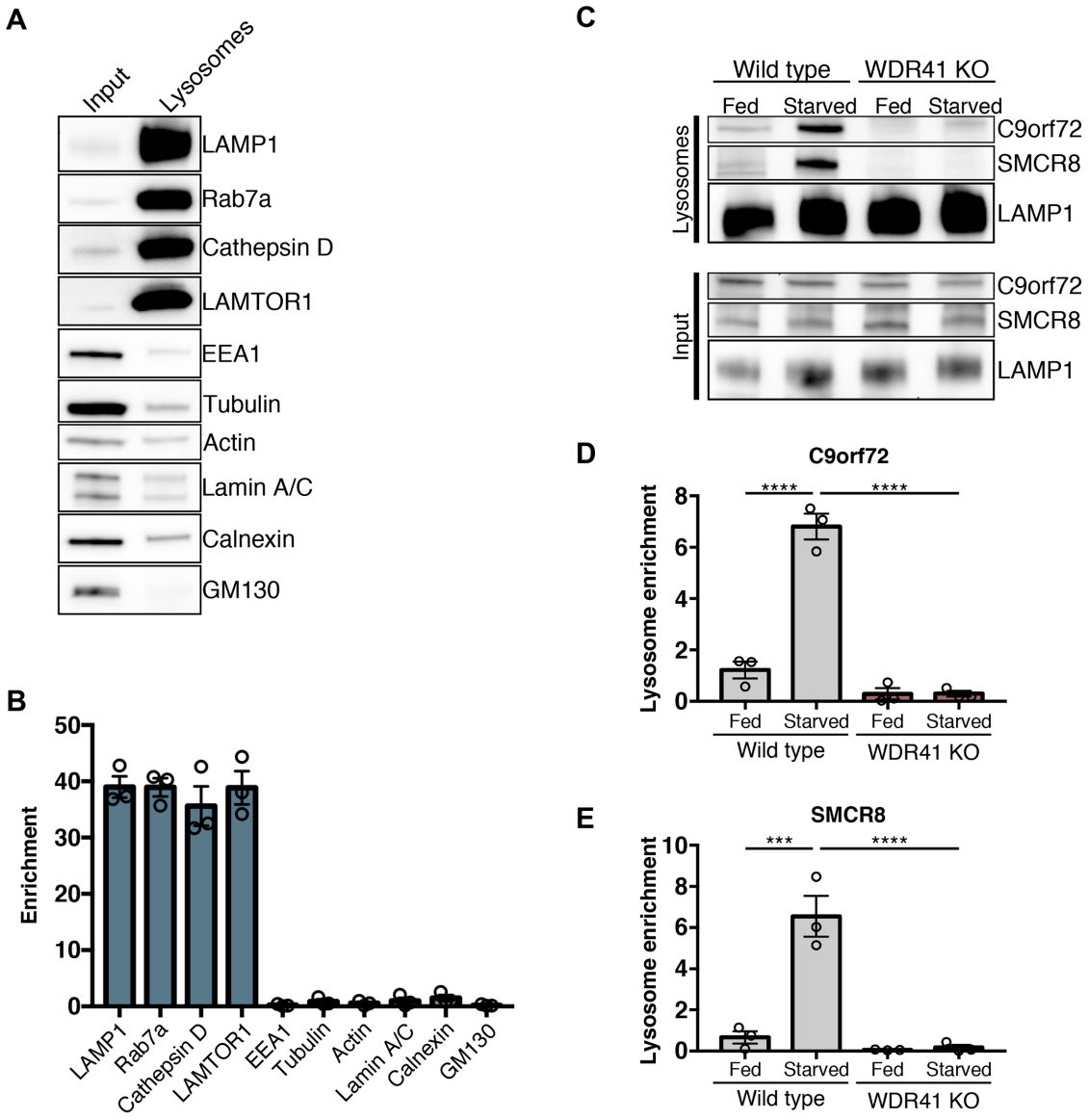

FIGURE 3: WDR41 is required for C9orf72 and SMCR8 enrichment on purified lysosomes. (A) Immunoblots of the indicated proteins in the total cell lysate (input) and in magnetically isolated lysosomes (lysosomes). Equal amounts of protein were loaded in each lane. LAMP1, Rab7a, Cathepsin D (mature form), and LAMTOR1 were used as markers of late endosomes/lysosomes; EEA, early endosomes; tubulin, actin, cytoskeleton; Lamin A/C, nucleus; Calnexin, ER; GM130, –Golgi. (B) Quantification of immunoblots for the indicated proteins expressed as a fold increase in the lysosome fraction relative to the input (mean ± SEM, $n = 3$). (C) Immunoblots of C9orf72, SMCR8, and LAMP1 in the total cell lysate (input) and in magnetically isolated lysosomes under fed and starved conditions in wild-type and WDR41 KO HeLa cells. Quantification of the levels of C9orf72 (D) and SMCR8 (E) on magnetically isolated lysosomes (mean ± SEM, $n = 3$, ****$p < 0.0001$, ***$p \leq 0.001$ two-way analysis of variance [ANOVA] with Tukey's multiple comparisons test).

gene in HEK293FT cells. DNA sequencing and anti-HA immunofluorescence established the success of this strategy (Figure 4, A and B). We also confirmed that the addition of the 2xHA tag did not interfere with the ability of WDR41 to interact with C9orf72 and SMCR8 (Figure 4C). While immunofluorescence analysis of WDR41-2xHA cells under basal growth conditions (fed) revealed a diffuse staining pattern without obvious enrichment on lysosomes, WDR41 colocalized with LAMP1, an abundant integral membrane protein of lysosomes, in response to starvation (Figure 4D). The enhanced lysosome localization of WDR41 in starved cells was independently confirmed by immunoblot analysis of magnetically purified lysosomes (Figure 4, E and F). Thus, while WDR41 was previously reported to localize to the Golgi based on analysis of cells that overexpressed GFP-tagged WDR41 (Sullivan *et al.*, 2016), we now provide new data based on analysis of the endogenously expressed protein via two independent methods that instead establishes lysosomes as a major site of enrichment for WDR41.

Lysosome localization of WDR41 is independent of autophagy and the ULK complex

In contrast to the robust lysosome localization for WDR41 in starved cells, we did not observe enrichment of WDR41 on the LC3-positive autophagosomes that form under starvation conditions (Figure 5, A and B). This selectivity of WDR41 for localization to lysosomes rather

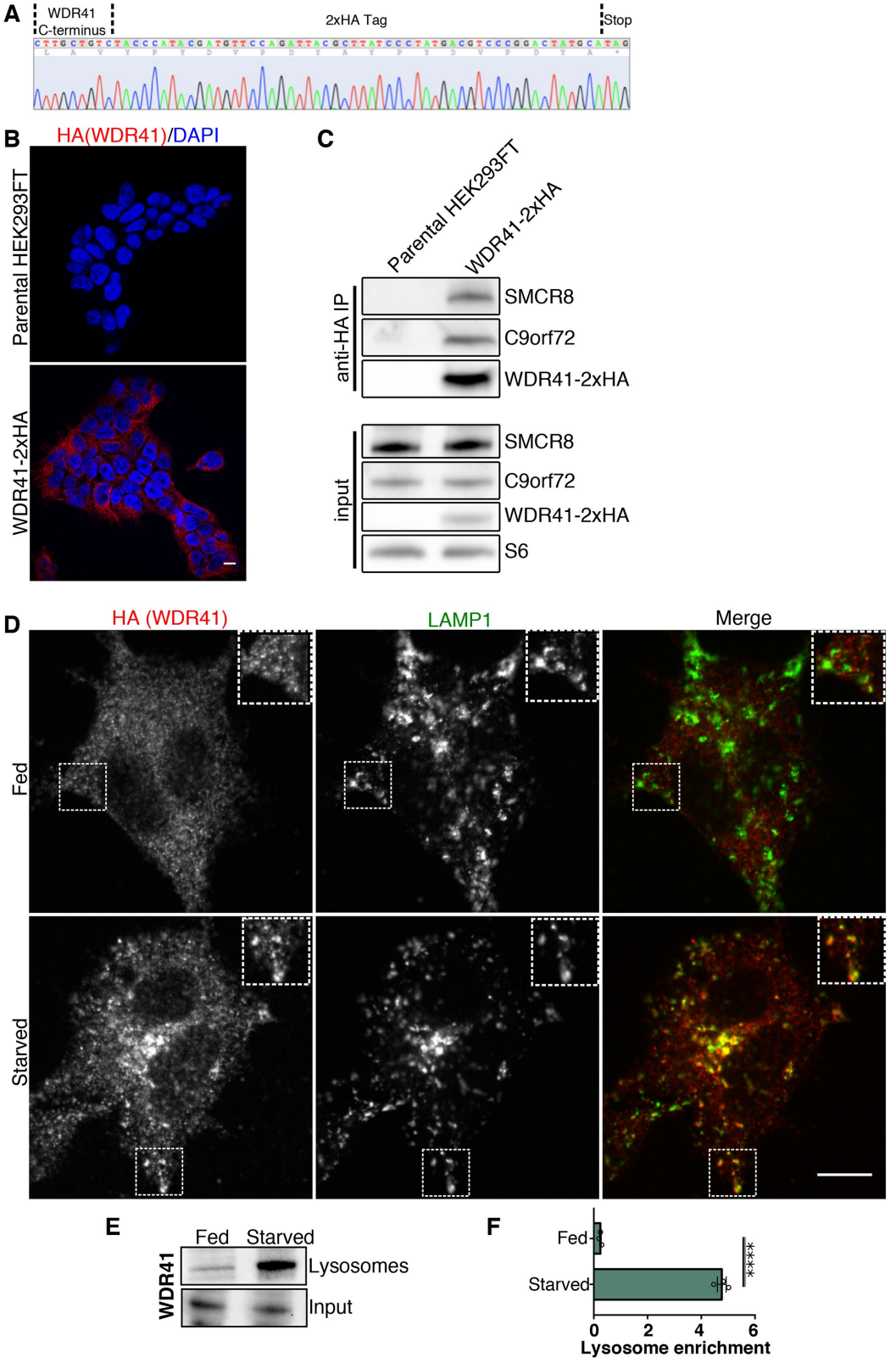

FIGURE 4: WDR41 localizes to lysosomes in starved cells. (A) Sequencing result from the genomic DNA PCR product from HEK293FT cells that have a 2xHA epitope tag inserted at the endogenous WDR41 locus. The positions of the WDR41 C-terminal sequence, 2xHA epitope tag, and stop codon are indicated. (B) The specificity of the anti-HA immunofluorescence signal in WDR41-2xHA cells is supported by the absence of this signal in parental, non-gene-edited cells. Scale bar, 10 μm. (C) Anti-HA immunoprecipitations from WDR41-2xHA cells followed by immunoblotting for the indicated proteins. WDR41-2xHA retains the ability to interact with C9orf72 and SMCR8. Non-gene-edited HEK293FT cells served as a negative control. (D) Immunofluorescence images showing the localization of WDR41-2xHA (expressed

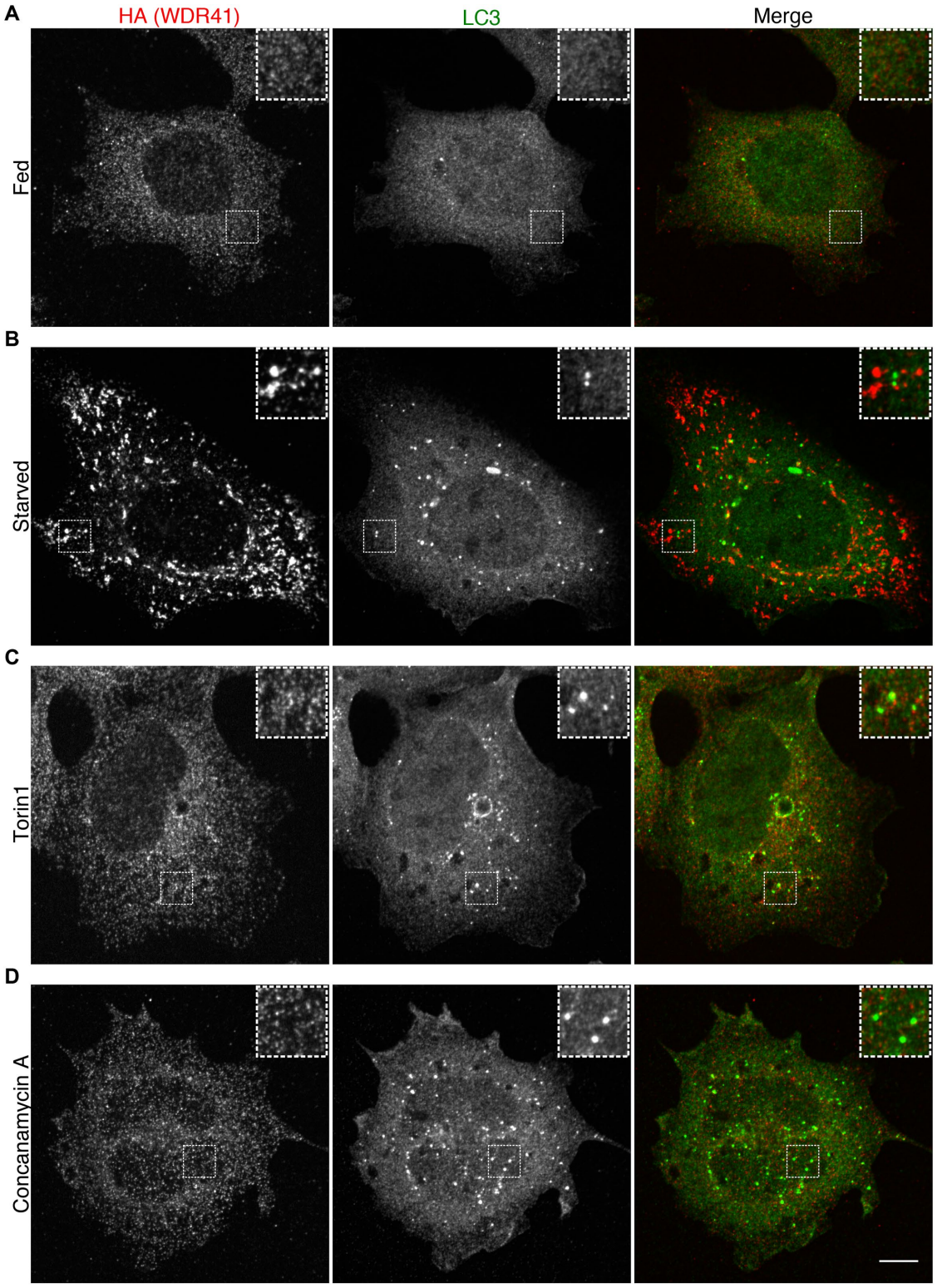

FIGURE 5: WDR41 is selectively recruited to lysosomes in response to starvation. Immunofluorescence images showing the localization of endogenously expressed WDR41-2xHA in (A) fed, (B) starved (1.5-h serum and amino-acid-free conditions), (C) torin1-treated (2 μM, 2 h), and (D) concanamycin A-treated (1 μM, 2 h). Scale bar, 10 μm.

from the endogenous locus) and LAMP1 in fed and starved (1.5-h serum and amino-acid-free) conditions. (E) Immunoblot analysis of WDR41 levels on magnetically-isolated lysosomes from HeLa cells in fed and starved conditions. (F) Quantification of WDR41 immunoblots expressed as a fold increase in the lysosome fraction relative to the input (mean ± SEM, $n = 3$, unpaired t test, ****$p < 0.0001$).

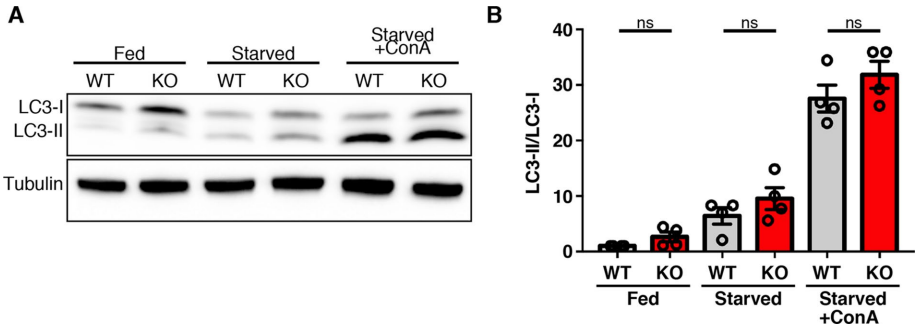

FIGURE 6: LC3 lipidation and autophagic flux is unimpaired in WDR41 KO cells. (A) Immunoblot analysis of LC3 levels in wild-type and WDR41 knockout cells under fed, starved, and starved cells treated with the v-ATPase inhibitor concanamycin A (ConA). (B) Quantification of LC3-II/tubulin levels (mean ± SEM, $n = 4$, Sidak's multiple comparisons test).

than autophagosomes parallels previous observations for C9orf72 (Amick *et al.*, 2016). Further supporting the conclusion that WDR41 recruitment to lysosomes in starved cells is not dependent on autophagy are observations that WDR41 subcellular localization does not change in cells where autophagosomes accumulate due to either mTOR inhibition with torin 1 (Figure 5C) or V-ATPase inhibition with concanamycin A (Figure 5D). Collectively, these results demonstrate that WDR41 is selectively recruited to lysosomes in response to starvation but does not reflect a general response to increased autophagosome abundance.

The distinction between autophagosome versus lysosome-localized actions of WDR41, C9orf72, and SMCR8 is important in light of previous studies that have implicated these proteins in the process of autophagy (Sellier *et al.*, 2016; Sullivan *et al.*, 2016; Ugolino *et al.*, 2016; Webster *et al.*, 2016; Yang *et al.*, 2016; Jung *et al.*, 2017). To further investigate the relationship between WDR41 and autophagy induction, we examined LC3 lipidation (a key step in the induction of autophagy) via immunoblotting of cells that were starved in the absence and presence of concanamycin A to discriminate between autophagy and subsequent lysosome-mediated clearance (Figure 6A). LC3 lipidation was increased to a similar extent in both wild type (WT) and WDR41 KO cells in response to starvation. Likewise, the measurement of autophagic flux via analysis of cells that were starved in the presence of concanamycin A also revealed no significant defect in the WDR41 KO cells (Figure 6, A and B). These results demonstrate that WDR41 is not essential for autophagy.

Aside from WDR41, the other major known interactor of C9orf72 and SMCR8 is the ULK complex that contains the ULK, RB1CC1, ATG13, and ATG101 proteins (Sullivan *et al.*, 2016; Webster *et al.*, 2016; Yang *et al.*, 2016; Jung *et al.*, 2017). ULK phosphorylates substrates to promote autophagy induction (Russell *et al.*, 2013). Interactions between the C9orf72 and ULK complexes suggested that, like WDR41, the ULK complex could also be required for C9orf72 recruitment to lysosomes. Therefore, we next investigated the contribution of the ULK complex to lysosome recruitment of C9orf72 via depletion of RC1CC1 (also known as FIP200, an essential subunit of the ULK complex) (Hara *et al.*, 2008). These experiments were performed in the 2xHA-C9orf72 293FT cell line to take advantage of robust assays that we have developed for imaging C9orf72 subcellular localization in these cells (Amick *et al.*, 2016). CRISPR-Cas9-mediated targeting of the RB1CC1 locus resulted in RB1CC1 protein depletion (Figure 7A) and severely impaired autophagic flux (Figure 7, B and C). However, in contrast to the loss of C9orf72 recruitment to lysosomes that we observed in WDR41 KO cells (Figure 2), C9orf72 still accumulated on lysosomes in response to starvation in the RB1CC1 mutant cells (Figure 7D). Conversely, double labeling for C9orf72 and LC3 confirmed that starvation-induced C9orf72 puncta occurred even in the absence of detectable LC3-positive autophagosome formation (Figure 7E). These results indicate that recruitment of the C9orf72 complex to lysosomes is not dependent on autophagy or ULK complex function and that it is also unlikely that C9orf72 transits to lysosomes via autophagosomes. In addition, these data concerning RB1CC1 further emphasize the specificity of WDR41 contributions to the lysosome localization of the C9orf72 complex.

WDR41 supports mTORC1 activation by amino acids

We and others have documented a role for C9orf72 and SMCR8 in the regulation of mTORC1 signaling (Amick *et al.*, 2016; Ugolino *et al.*, 2016; Yang *et al.*, 2016; Amick and Ferguson, 2017; Jung *et al.*, 2017). As the loss of C9orf72 lysosome localization in WDR41 KO cells suggested a requirement for WDR41 in supporting normal mTORC1 signaling, we next tested whether WDR41 KO cells are able to efficiently activate mTORC1 in response to an acute amino acid stimulus. In contrast to control cells that robustly activate mTORC1 upon stimulation with amino acids (as read out by phosphorylation of threonine 389 on ribosomal protein S6 kinase [S6K]), this response was severely impaired in WDR41 KO cells (Figure 8, A and B). The specificity of the mTORC1 signaling defect in WDR41 KO cells is supported by the rescue of this phenotype following the lentivirus-mediated reexpression of HA-tagged WDR41 (Figure 8, A and B). This result also confirms that C-terminal HA-tags do not inhibit WDR41 function and thereby provides additional validation for our interpretation of localization results for the WDR41-2xHA protein.

Constitutive targeting of C9orf72 to lysosomes overcomes the need for WDR41

The C9orf72-SMCR8 localization and mTORC1 regulation defects in WDR41 KO cells raised questions about the function of WDR41 at lysosomes. Is WDR41 simply required for the efficient recruitment of C9orf72 and SCMR8 to lysosomes? Or does WDR41 itself also contribute to the activation of mTORC1? To answer these questions, we constitutively targeted C9orf72-GFP to lysosomes by fusing it to the first 39 amino acids of LAMTOR1 (we refer to this fusion protein as Lyso-C9orf72-GFP, Figure 8C). This region of LAMTOR1 is lipidated and has been previously demonstrated to support the targeting of fusion proteins to lysosomes (Nada *et al.*, 2009; Sancak *et al.*, 2010; Menon *et al.*, 2014). We tested the lysosome localization of lyso-C9orf72-GFP in WDR41 KO cells and found that it robustly localized to lysosomes that were visualized with cresyl violet (Figure 8D), a dye that selectively labels lysosomes based on the acidic pH of their lumen (Ostrowski *et al.*, 2016). Lyso-C9orf72-GFP also retains the ability to interact with SMCR8 (Supplemental Figure S2).

Having validated the successful WDR41-independent targeting of C9orf72 to lysosomes, we next tested the ability of this fusion protein to support mTORC1 signaling and observed that lysosome-targeted C9orf72 partially restored amino acid responsiveness of mTORC1 activity in WDR41 KO cells (Figure 8, E and F). These results indicate that a major function for WDR41 is to support the recruitment of C9orf72 and SMCR8 to lysosomes. Furthermore, although constitutive targeting of C9orf72 to lysosomes

rescues mTORC1 signaling in WDR41 KO cells, such signaling remains responsive to starvation and amino acid refeeding. The Rag GTPases are well characterized as targets of multiple amino acid sensing pathways and in turn recruit mTORC1 to lysosomes when amino acids are plentiful (Saxton and Sabatini, 2017). We did not observe any impact of WDR41 on the lysosomal localization of RagC under either starved or fed conditions (Supplemental Figure S3, A and B). Likewise, mTOR also showed a normal pattern of amino acid regulated lysosome recruitment in WDR41 KO cells (Supplemental Figure S4, A and B). This matches what we previously observed for regulation of mTOR localization in C9orf72 and SMCR8 KO cells (Amick *et al.*, 2016). Thus, the complex of C9orf72-SMCR8-WDR41 is critical for making lysosomes permissive for supporting the activation of mTORC1 by amino acids but does not overcome the requirement for amino acids in supporting mTORC1 signaling.

DISCUSSION

WDR41 functions at lysosomes

Although data from several labs previously identified WDR41 as an interacting partner of C9orf72 (Sellier *et al.*, 2016; Sullivan *et al.*, 2016; Xiao *et al.*, 2016; Yang *et al.*, 2016; Jung *et al.*, 2017), its role in the larger C9orf72 complex was not defined. In this study, we show that WDR41 is a constitutive member of this heterotrimeric complex and is essential for the regulated recruitment of C9orf72 and SMCR8 to lysosomes. The absence of C9orf72 and SMCR8 localization to lysosomes during starvation and impaired mTORC1 activation by amino acids in WDR41 KO cells establishes an important role for WDR41 in this larger protein complex. The specific contribution of WDR41 to the function of the complex was further dissected by developing a strategy to restore targeting of C9orf72-SMCR8 localization to lysosomes in WDR41 KO cells. In such cells, mTORC1-responsiveness to amino acids was improved. We thus conclude that WDR41 plays an essential role in the regulated lysosomal targeting of C9orf72-SMCR8 but is not required for their subsequent ability to support mTORC1 signaling.

The subcellular localization of a protein is a critical determinant of its function. We now provide multiple lines of evidence that identify lysosomes as a major site of WDR41 enrichment and function. Key data include immunofluorescence localization of endogenously expressed HA-tagged WDR41, immunoblot analysis of purified lysosomes, and the impact of WDR41 KO on the lysosome recruitment of both C9orf72 and SMCR8. Further support for the conclusion that WDR41 undergoes regulated recruitment to lysosomes as part of a complex with C9orf72 and SMCR8 is provided by a recent proteomic analysis that detected enhanced lysosome abundance of C9orf72, SMCR8, and WDR41 as part of a large-scale proteomic analysis of subcellular fractions from the livers of fed versus starved rats (Jadot *et al.*, 2017). These in vivo observations indicate that our observations concerning C9orf72, SMCR8, and WDR41 lysosome localization in cultured cells can be generalized to a broader range of physiological contexts.

Role of WDR41 in the lysosomal recruitment of the C9orf72 complex

With the discovery that WDR41 is required for the regulated recruitment of C9orf72 and SMCR8 to lysosomes, questions arise concerning the specific mechanisms that allow WDR41 to perform such a function. WDR41 is predicted to contain between six and eight WD repeats spanning the bulk of its primary sequence (Wang *et al.*, 2015; Amick and Ferguson, 2017). Aside from these WD repeats, WDR41 contains only short regions that are predicted to lack secondary structure (Wang *et al.*, 2015; Amick and Ferguson, 2017). Structural studies of other WD repeat proteins showed that they typically form seven-bladed β-propellers (Wall *et al.*, 1995; Bajagic *et al.*, 2017). These β-propellers function as scaffolds that often provide multiple interaction surfaces for the assembly of larger protein complexes and that can also support protein–membrane interactions (Dove *et al.*, 2004; Jeffries *et al.*, 2004; Stirnimann *et al.*, 2010). As our data did not reveal an essential role for WDR41 in supporting the interaction between C9orf72 and SMCR8, we instead predict a possible interaction between WDR41 and a protein or lipid on the surface of lysosomes that could contribute to the regulated recruitment of C9orf72 and SMCR8 to lysosomes. An interesting example that has some parallels to the combination of DENN domains and WD repeat motifs in the C9orf72-SMCR8-WR41 complex is the Rab12 guanine nucleotide exchange factor (GEF) known as DENND3 that contains both a DENN domain as well as WD repeats (Xu and McPherson, 2017). This raises the possibility of a more broadly conserved functional interplay between DENN domains and WD-repeat β-propellers. While our study identifies a function for WDR41, the specific contributions of C9orf72 and SMCR8 to overall complex function remain to be elucidated. Double depletion of both C9orf72 and SMCR8 ameliorates the defects in mTORC1 signaling that were observed in single C9orf72-depleted cells, suggesting SMCR8 gain-of-function could be responsible for some C9orf72 knockout phenotypes (Amick *et al.*, 2016; Yang *et al.*, 2016). Indeed, independent functions of SMCR8 were recently reported (Jung *et al.*, 2017).

Relationship between the C9orf72 complex and mTORC1 signaling

The WDR41-dependent recruitment of C9orf72 and SMCR8 to lysosomes occurs most prominently when cells are starved of amino acids. This indicates the need for mechanisms that sense changes in nutrient availability and transduce this information into changes at lysosomes that can be read out by WDR41. The best characterized example of a lysosome-localized signaling pathway that is responsive to changes in nutrient availability is mTORC1 (Saxton and Sabatini, 2017). The regulation of mTORC1 signaling by changes in amino acid availability occurs via regulation of the nucleotide status of the Rag GTPases. The Rags function as heterodimers composed of RagA or RagB bound to RagC or RagD that localize to the surface of late endosomes and lysosomes (Sancak *et al.*, 2010). The active form of Rag heterodimers that recruits mTORC1 to the surface of lysosomes consists of GTP-bound RagA/B and GDP-bound RagC/D. The nucleotide status of the Rags is regulated by amino acid availability via several sensors that function within signal transduction cascades that control the nucleotide state of the Rags (Wolfson and Sabatini, 2017). Altogether, these mechanisms ensure that mTORC1 recruitment to lysosomes and subsequent activation only efficiently occurs when amino acids are abundant. Interestingly, although the C9orf72-SCMR8-WDR41 complex is acutely recruited to lysosomes in response to amino acid depletion and is required for subsequent activation of mTORC1 on amino acid refeeding, these proteins do not bind to the Rags and are not required for the Rag-dependent enrichment of mTORC1 on lysosomes (Supplemental Figures S3 and S4) (Amick *et al.*, 2016; Amick and Ferguson, 2017). Likewise, constitutive targeting of C9orf72 to lysosomes restores amino acid stimulation of mTORC1 signaling to WDR41 KO cells but does obviate the need for amino acids activate mTORC1 signaling. Based on these factors, it is possible that the C9orf72 complex may function as part of a novel, lysosome-localized, pathway that contributes to cellular adaptation to changes in nutrient availability that functions

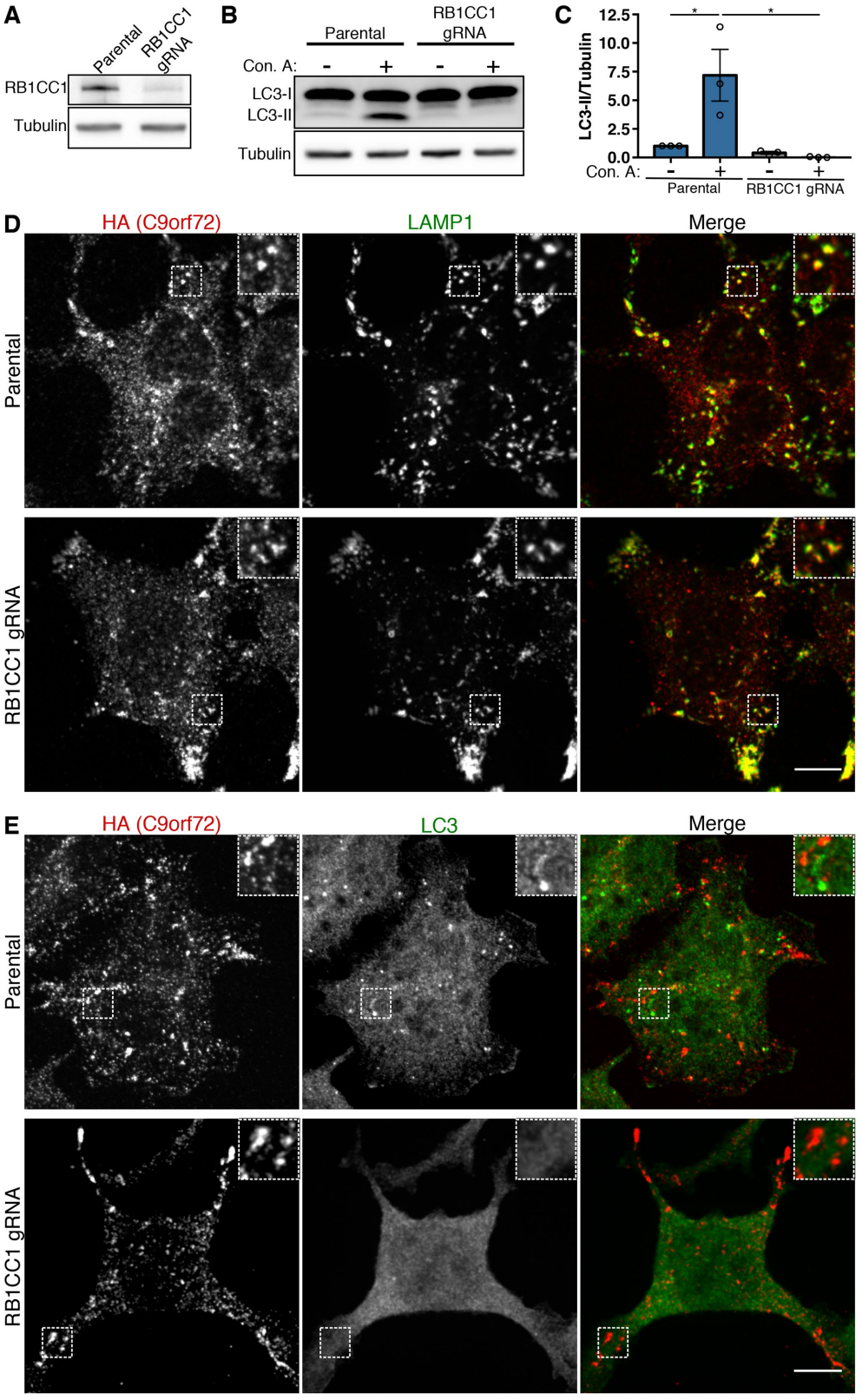

FIGURE 7: RB1CC1 and autophagy are not required for C9orf72 recruitment to lysosomes. (A) Immunoblot analysis of CRISPR-Cas9-mediated RB1CC1 depletion in the HEK293FT cell line that expresses 2xHA-C9orf72 from the endogenous locus. (B) Parental 2xHA-C9orf72 HEK293FT and RB1CC1-depleted cells were treated with and without concanamycin A (V-ATPase inhibitor) for 2 h and autophagic flux was assessed by immunoblotting. Although wild-type cells accumulate LC3-II when treated with concanamycin A, the RB1CC1-depleted cell line does not. (C) Quantification of the ratio of LC3-II to tubulin (mean ± SEM, $n = 3$, $^*p \leq 0.05$, two-way ANOVA with Tukey's multiple comparisons test). (D) Immunofluorescence analysis of C9orf72 localization in starved wild-type and RB1CC1-depleted cells. Scale bar,

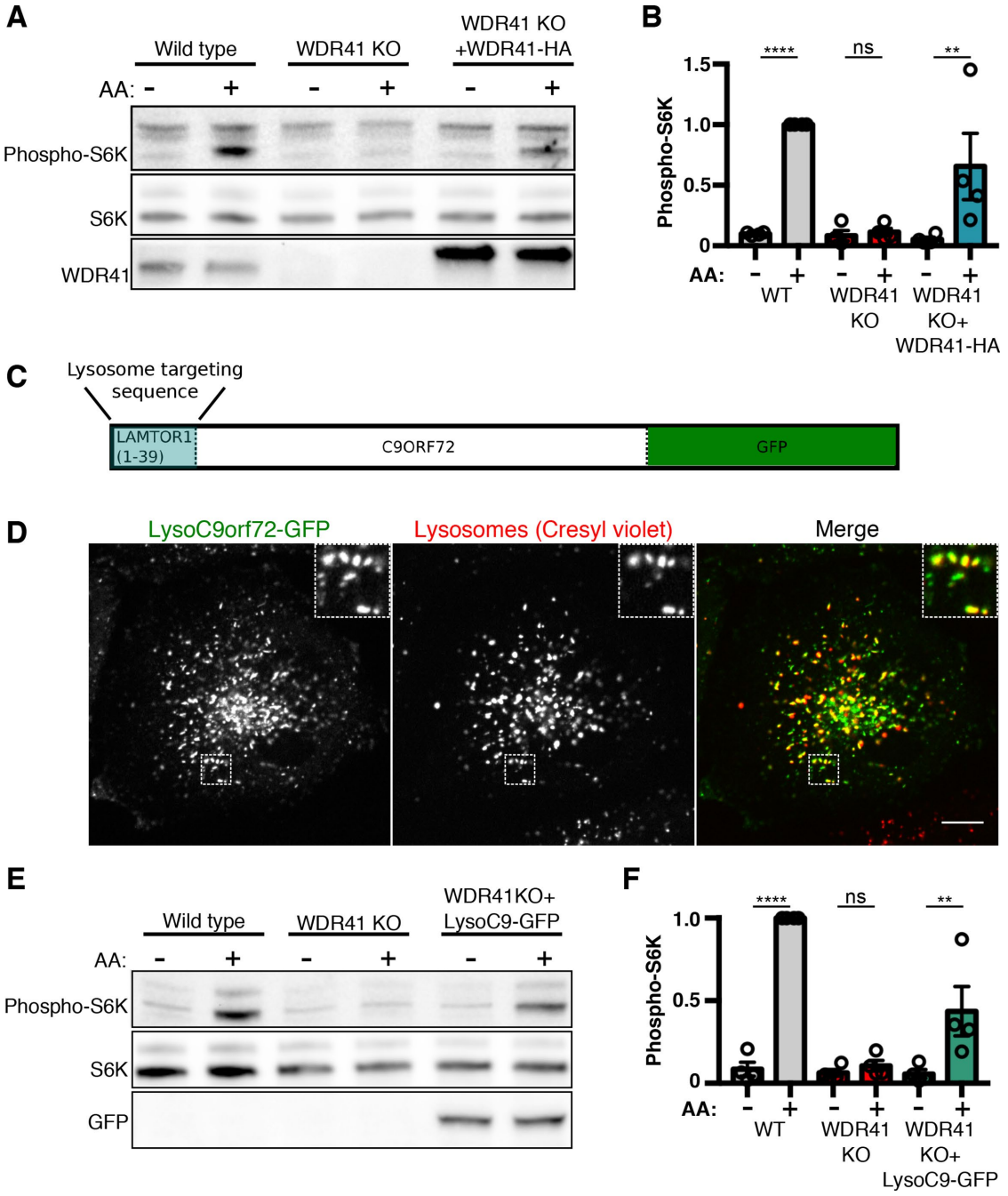

FIGURE 8: WDR41-dependent recruitment of C9orf72 to lysosomes is critical for the stimulation of mTORC1 activity by amino acids (A) Immunoblot analysis of phospho-S6 kinase (S6K-T389) levels during starvation (1.5 h) and subsequent amino acid (AA) refeeding (15 min) in WT, WDR41 knockout, and cells stably expressing WDR41-HA in the WDR41 knockout background. (B) Summary of S6 kinase phosphorylation levels normalized to total S6K levels; WT refeed normalized to 1 (mean ± SEM, $n = 4$, ****$p < 0.0001$, **$p \leq 0.01$, ANOVA with Sidak's multiple comparisons test). (C) Schematic diagram of the Lyso-C9orf72-GFP construct. The first 39 amino acids of LAMTOR1 were fused to the N-terminus of C9orf72 followed by a C-terminal GFP tag. (D) Live-cell imaging reveals the successful targeting of Lyso-C9orf72-GFP to lysosomes as illustrated by colocalization with cresyl violet, a fluorescent reporter of lysosome acidity. Scale bar = 10 μm. (E) Immunoblot analysis of phospho-S6K levels during starvation (1.5 h) and subsequent AA refeeding (15 min) in wild-type, WDR41 knockout, and cells stably expressing Lyso-C9orf72-GFP in the WDR41 knockout background. (F) Quantification of S6K phosphorylation levels normalized to total S6K levels (WT refeed normalized to 1; mean ± SEM, $n = 4$, ****$p < 0.0001$, **$p \leq 0.01$, ANOVA with Sidak's multiple comparisons test).

10 μm. (E) Immunofluorescence analysis of C9orf72 and LC3 in starved wild-type and RB1CC1-depleted cells. Starved wild-type cells have distinct C9orf72 and LC3 puncta (predominantly autophagosomes), while RB1CC1-depleted cells maintain C9orf72 puncta but lack LC3 puncta. Scale bar, 10 μm.

in parallel to the better characterized mechanisms that converge on the Rags.

ULK complex is not required for lysosome localization of C9orf72

The identification of interactions between the C9orf72 and ULK complexes previously gave rise to the concept that C9orf72, SMCR8, and WDR41 play a role in the process of autophagy due to the involvement of ULK in autophagy initiation (Sellier *et al.*, 2016; Sullivan *et al.*, 2016; Xiao *et al.*, 2016; Yang *et al.*, 2016; Jung *et al.*, 2017). The starvation conditions that stimulate C9orf72 complex recruitment to lysosomes also induce autophagy. In this study, we have used genetic and pharmacological perturbations to distinguish between these processes. Our new data show that when autophagosomes accumulate in response to mTOR and V-ATPase inhibition, there is no parallel change in the subcellular localization of WDR41. Furthermore, C9orf72 still builds up on lysosomes in response to starvation even in cells where autophagy has been suppressed by RB1CC1 depletion. This indicates that the recruitment of the C9orf72 complex to lysosomes is not a secondary consequence of either mTOR inhibition or autophagy induction. Instead, this complex appears to be responding more directly to changes in amino acid availability. Collectively, these results suggest the existence of a novel nutrient sensing mechanism that functions upstream of the C9orf72 complex but that does not require the Rag GTPases, mTORC1, or the ULK complex.

C9orf72 haploinsufficiency and ALS–FTD pathogenesis

Significant interest into the function of C9orf72 (and by extension SMCR8 and WDR41) has been stimulated by the potential role played by C9orf72 haploinsufficiency in ALS–FTD disease pathogenesis (Shi *et al.*, 2018). Our new findings solidify the role played by lysosomes as a major subcellular site of action for the C9orf72-SMCR8-WDR41 complex. They furthermore indicate that the lysosome dysfunction in macrophages and microglia from C9orf72 KO mice likely results from the direct loss of normal C9orf72 complex function at lysosomes (O'Rourke *et al.*, 2016). Contributions of lysosome dysfunction to ALS–FTD risk are both plausible and interesting given human genetic studies that have implicated multiple genes related to endolysosome function such as GRN, SQSTM1, CHMP2B, OPTN, and TBK1 as risk factors for these diseases (Skibinski *et al.*, 2005; Baker *et al.*, 2006; Cruts *et al.*, 2006; Maruyama *et al.*, 2010; Fecto *et al.*, 2011; Rubino *et al.*, 2012; Freischmidt *et al.*, 2015). However, as important as it is to determine the putative relevance of C9orf72 deficiency to ALS–FTD disease mechanisms, the lysosome-related functions of the C9orf72-SMCR8-WDR41 complex and its role in matching lysosome function to ongoing changes in nutrient availability are of broad cell biological interest that extends beyond putative neurodegenerative disease mechanisms.

Conclusion

In summary, our new findings establish important lysosome-localized functions for WDR41 and provide a foundation for future studies focused on the further elucidation of both the functions of the C9orf72–SMCR8–WDR41 protein complex as well as lysosome-localized mechanisms that support its regulation by changes in amino acid availability.

MATERIALS AND METHODS

Cell culture and transfection

HEK293FT (Life Technologies, Carlsbad, CA) and HeLa cells (provided by P. De Camilli, Yale University, New Haven, CT) were grown in high-glucose DMEM (+L-glutamine), 10% fetal bovine serum (FBS), and 1% penicillin/streptomycin supplement (Invitrogen, Carlsbad, CA). Where indicated, cells were starved for 90 min by incubation with amino acid–free Roswell Park Memorial Institute (RPMI) media (US Biological, Swampscott, MA). Amino acid refeeding was performed with 1 × MEM amino acid supplement (Invitrogen) added to starvation medium for 15 min. For starvation/refeeding assays in Figure 5, 500,000 HeLa cells were seeded in 10-cm dishes for 24 h prior to the start of the experiment. Transfections were performed with 500 ng of DNA, 100 µl of OptiMEM (Invitrogen), and 1.5 µl of FuGENE 6 transfection reagent (Promega, Madison, WI) per 35-mm dish and scaled up proportionately for larger and smaller dishes. For transient transfections, cells were analyzed 2 d posttransfection.

CRISPR/Cas9 genome editing

Guide RNAs were designed using the CRISPR design tool (crispr.mit.edu) or selected from predesigned guide RNA sequences (Wang *et al.*, 2014). Guide RNA–encoding DNA oligonucleotides (IDT) were annealed and ligated into *Bbs*1-digested pX459 vector (acquired from Feng Zhang [Massachusetts Institute of Technology] via Addgene) and transformed into Stabl3-competent *Escherichia coli* cells (Ran *et al.*, 2013). Oligonucleotide sequences used for this purpose are described in Supplemental Table 1. Successful insertion of the guide RNA–encoding DNA sequence was confirmed by sequencing. Plasmids (0.4 µg) were transfected with FuGENE 6 into 35,000 HeLa or 250,000 HEK293FT cells per well of a six-well dish. The next day, transfected cells were selected with puromycin for 3 d (2 µg/ml for HeLa, 1.25 µg/ml for HEK293FT). Surviving cells were subsequently plated at clonal density. Following the selection and expansion of colonies, KOs were identified by immunoblotting and subsequently confirmed by sequencing of PCR-amplified genomic DNA. To sequence genomic DNA, it was extracted (QuickExtract DNA extraction solution; Epicentre Biotechnologies), and the region of interest was amplified by PCR (primers described in Supplemental Table 1), cloned into the pCR-Blunt TOPO vector (Zero Blunt TOPO PCR cloning kit; ThermoFisher Scientific), and transformed into TOP10-competent *E. coli* cells. Plasmid DNA was then isolated from multiple colonies and sequenced to define the genotype of the locus of interest. To generate RB1CC1-depleted cells, 2xHA-C9orf72 HEK293FT cells were transfected with a pair of px459 plasmids encoding guide RNAs targeting exons 1 and 2 of RB1CC1. Puromycin treatment and clonal selection was then performed as described above.

Our method for CRISPR/Cas9 genome editing for the insertion of epitope tags at endogenous loci was described previously (Petit *et al.*, 2013). The single-strand DNA oligonucleotide (ssODN) homology-directed repair donor template was designed with asymmetric homology arms on the PAM proximal and distal sides of the cut site to enhance the efficiency of tag insertion (Richardson *et al.*, 2016). The specific guide RNA and ssODN repair template sequences (IDT) that were used to insert the 2xHA epitope tag into the WDR41 gene are provided in Supplemental Table 2. CRISPR ribonucleoprotein (RNP) complexes and the ssODN repair template were delivered to cells by nucleofection (Leonetti *et al.*, 2016). To assemble the RNPs, crRNA and tracrRNA (IDT) were mixed at a 1:1 ratio (50 µM final concentration of each) and heated at 95°C for 5 min and then cooled to room temperature. This RNA duplex (150 pmol) was then added to 150 pmol Cas9 protein (IDT), and the volume was adjusted to 10 µl with Opti-MEM. Three microliters of 100 µM ssODN repair donor template was then added. The RNP complex+ssODN was added to nucleofection buffer and nucleofected into 1 million HEK293FT cells (Kit R, electroporation program A24; Lonza, Basel, Switzerland).

Clonal cell populations were subsequently isolated from these cells and screened for HA signal by immunoblotting and immunofluorescence. To confirm further the correct in-frame insertion of the 2xHA tag in these cells, genomic DNA surrounding the site of tag insertion was PCR amplified and sequenced as described above.

Immunoprecipitation and immunoblotting

Cells were washed with ice-cold phosphate-buffered saline (PBS), lysed in Tris-buffered saline (TBS) plus 1% Triton X-100 plus protease and phosphatase inhibitor cocktails (Roche Diagnostics, Indianapolis IN), and insoluble material was cleared by centrifugation for 10 min at 20,000 × *g*. Immunoprecipitations were performed on the resulting lysates. For anti-GFP immunoprecipitations, GFP-Trap resin (ChromoTek, Planegg-Martinsried, Germany) was incubated with lysates for 2 h with rotation at 4°C, followed by five washes with lysis buffer and elution in 2× Laemmli buffer. For anti-HA immunoprecipitations, anti-HA Affinity Matrix (Roche Diagnostics) was used. Immunoblotting was performed with 4–15% gradient Mini-PROTEAN TGX precast polyacrylamide gels and nitrocellulose membranes (Bio-Rad, Hercules CA). Blots were blocked with 5% milk, and antibodies were incubated with 5% milk or bovine serum albumin in TBS with 0.1% Tween 20. Chemiluminescence detection of horseradish peroxidase signals from secondary antibodies was performed on a VersaDoc imaging station (Bio-Rad). Antibodies used in this study are listed in Supplemental Table 3.

Plasmids

GFP-tagged full-length C9orf72 (residues 1–481, Uniprot identifier Q96LT7-1) and SMCR8 (residues 1–937, Uniprot identifier Q8TEV9-1) were described previously (Amick *et al.*, 2016). pCMV6 WDR41-HA was a gift from Nicolas Charlet-Berguerand, Université de Strasbourg, Illkirch, France (Addgene plasmid #74159) (Sellier *et al.*, 2016). Full-length WDR41 (residues 1–459) and WDR41-HA were PCR amplified from this vector. An upstream open reading frame was included prior to the start codon to reduce the extent of WDR41 overexpression (Ferreira *et al.*, 2013). PCR products were then cloned into *Sma*I-digested pLVX-Puro vector (Clontech) by Gibson Assembly. To generate the LAMTOR1 (residues 1–39)-C9orf72-GFP fusion construct (lyso-C9orf72-GFP), the relevant fragments of LAMTOR1 and C9orf72 were amplified by PCR and joined by Gibson Assembly with the pEGFPN1 vector (Clontech); the lyso-C9orf72-GFP sequence was then amplified by PCR and joined by Gibson Assembly with the pLVX-Puro vector. Expression of GFP alone was achieved by transfection of the pEGFPC2 plasmid (Clontech). Oligonucleotide primer sequences used to generate these plasmids are listed in Supplemental Table 1.

Lentivirus packaging and transduction

To stably express WDR41 in the background of WDR41 knockout cell lines, HEK293FT cells were transfected using Fugene 6 and the psPAX2, pCMV-VSVG, and pLVX-Puro-WDR41 plasmids. psPAX2 was a gift from Didier Trono, École polytechnique fédérale de Lausanne, Lausanne, Switzerland (Addgene plasmid # 12260); pCMV-VSV-G was a gift from Bob Weinberg, Whitehead Institute for Biomedical Research, Cambridge, MA (Addgene plasmid # 8454) (Stewart *et al.*, 2003). After 48 h, the viral supernatant was filtered through a 0.45-µm filter (Pall Corporation) onto the cells to be transduced. Polybrene solution (8 µg/ml; EMD Millipore, Darmstadt, Germany) was added to increase uptake of virus. Puromycin (Life Technologies by Life Technologies, Grand Island, NY; 2 µg/ml for HeLa, 1.25 µg/ml for HEK293FT) was then used to select for stable transductants.

Immunofluorescence and microscopy

Spinning disk confocal microscopy was performed using equipment described previously (Roczniak-Ferguson *et al.*, 2012). For immunofluorescence staining, cells were grown on 12-mm No. 1.5 coverslips (Carolina Biological Supply, Burlington NC) coated with poly-D-lysine (Sigma-Aldrich, Darmstadt, Germany) and fibronectin (EMD-Millipore). To fix cells, 8% paraformaldehyde (PFA) in 0.1 M sodium phosphate was added dropwise to cells in growth medium to achieve a final concentration of 4% PFA. Samples were fixed at room temperature for 30 min and then washed with PBS. Cells were permeabilized by immersing coverslips in ice-cold methanol for 3 s and then were blocked in 5% normal donkey serum (Jackson ImmunoResearch, West Grove, PA)/PBS for 1 h at room temperature. Subsequent antibody incubations were performed in this buffer. For immunofluorescence detection of 2xHA-tagged endogenous C9orf72 and WDR41, cells were first incubated with a mouse anti-HA antibody, followed by an unlabeled goat anti-mouse antibody, followed by an anti-goat fluorescent tertiary antibody. This approach was necessary to amplify the signal to detect these proteins at their low endogenous levels. Detection of other proteins by immunofluorescence was achieved by a traditional primary + fluorescent secondary antibody approach. Antibodies used in this study are listed in Supplemental Table 3. For live-cell imaging experiments, cells were imaged at room temperature in 10 mM HEPES, pH 7.4, 136 mM NaCl, 2.5 mM KCl, 2 mM $CaCl_2$, and 1.3 mM $MgCl_2$. Lysosomes were labeled with 1 µM cresyl violet (MP Biomedicals, LLC, Solon, OH) (Ostrowski *et al.*, 2016) for 10 min followed by a 10-min washout before imaging. Images were processed with ImageJ (National Institutes of Health). The percentage of starved cells with C9orf72 puncta colocalized with LAMP1 in Figure 2 was made by visual inspection of images from three independent experiments with >130 cells per cell line in total.

Magnetic isolation of lysosomes

Magnetic isolation of lysosomes with colloidal iron dextran (FeDex) nanoparticles was performed based on previously described protocols with several modifications (Walker and Lloyd-Evans, 2015; Tharkeshwar *et al.*, 2017). Briefly, cells were incubated for 24 h at 37°C with 10% FeDex nanoparticles that were synthesized by the coprecipitation method (Rodriguez-Paris *et al.*, 1993). After rinsing with PBS, cells were incubated with regular culture medium for 24 h. At the end of this chase period, the cells were rinsed and harvested in PBS, centrifuged (180 × *g*, 10 min), and homogenized in homogenizing buffer (HB; 250 mM sucrose, 5 mM Tris-HCl, and 1 mM egtazic acid (EGTA), pH 7.4, supplemented with protease inhibitors) using a ball-bearing cell cracker (20 passages at 10 µm clearance, Isobiotec, Germany). Following centrifugation at 800 × *g* for 10 min, the postnuclear supernatant was passed over an HB-equilibrated LS column (Miltenyi Biotec, Auburn, CA) placed inside a strong magnetic field (QuadroMACS Separator). Within the magnetic field, the nonmagnetic fraction was first removed by extensive washes with ice-cold HB. Next the LS column was removed from the magnetic field and the bound magnetic fraction containing the lysosomes was eluted in HB. Following a high-speed ultracentrifugation (126,000 × *g*, 1 h), the resulting lysosomal pellet was resuspended in HB, and the protein concentration was determined using the Bradford assay.

Statistical analysis

Data were analyzed using Prism (GraphPad Software). Error bars and tests are specified in the figure legends. Data distribution was assumed to be normal. However, this was not formally tested.

ACKNOWLEDGMENTS

We appreciate significant lab management contributions of Agnes Ferguson that broadly supported this project. Grants from the National Institutes of Health (NIH) (GM105718 and AG047270) and the Ellison Medical Foundation to S.F. provided financial support for this research. J.A. was supported by grants T32GM007223 and F31GM119249 from the NIH.

REFERENCES

Amick J, Ferguson SM (2017). C9orf72: At the intersection of lysosome cell biology and neurodegenerative disease. Traffic 18, 267–276.

Amick J, Roczniak-Ferguson A, Ferguson SM (2016). C9orf72 binds SMCR8, localizes to lysosomes, and regulates mTORC1 signaling. Mol Biol Cell 27, 3040–3051.

Baba M, Hong SB, Sharma N, Warren MB, Nickerson ML, Iwamatsu A, Esposito D, Gillette WK, Hopkins RF 3rd, Hartley JL, *et al.* (2006). Folliculin encoded by the BHD gene interacts with a binding protein, FNIP1, and AMPK, and is involved in AMPK and mTOR signaling. Proc Natl Acad Sci USA 103, 15552–15557.

Bajagic M, Archna A, Busing P, Scrima A (2017). Structure of the WD40-domain of human ATG16L1. Protein Sci 26, 1828–1837.

Baker M, Mackenzie IR, Pickering-Brown SM, Gass J, Rademakers R, Lindholm C, Snowden J, Adamson J, Sadovnick AD, Rollinson S, *et al.* (2006). Mutations in progranulin cause tau-negative frontotemporal dementia linked to chromosome 17. Nature 442, 916–919.

Belzil VV, Bauer PO, Prudencio M, Gendron TF, Stetler CT, Yan IK, Pregent L, Daughrity L, Baker MC, Rademakers R, *et al.* (2013). Reduced C9orf72 gene expression in c9FTD/ALS is caused by histone trimethylation, an epigenetic event detectable in blood. Acta Neuropathol 126, 895–905.

Corrionero A, Horvitz HR (2018). A C9orf72 ALS/FTD ortholog acts in endolysosomal degradation and lysosomal homeostasis. Curr Biol 22, 1522–1535.

Cruts M, Gijselinck I, van der Zee J, Engelborghs S, Wils H, Pirici D, Rademakers R, Vandenberghe R, Dermaut B, Martin JJ, *et al.* (2006). Null mutations in progranulin cause ubiquitin-positive frontotemporal dementia linked to chromosome 17q21. Nature 442, 920–924.

DeJesus-Hernandez M, Mackenzie IR, Boeve BF, Boxer AL, Baker M, Rutherford NJ, Nicholson AM, Finch NA, Flynn H, Adamson J, *et al.* (2011). Expanded GGGGCC hexanucleotide repeat in noncoding region of C9ORF72 causes chromosome 9p-linked FTD and ALS. Neuron 72, 245–256.

Dove SK, Piper RC, McEwen RK, Yu JW, King MC, Hughes DC, Thuring J, Holmes AB, Cooke FT, Michell RH, *et al.* (2004). Svp1p defines a family of phosphatidylinositol 3,5-bisphosphate effectors. EMBO J 23, 1922–1933.

Fecto F, Yan J, Vemula SP, Liu E, Yang Y, Chen W, Zheng JG, Shi Y, Siddique N, Arrat H, *et al.* (2011). SQSTM1 mutations in familial and sporadic amyotrophic lateral sclerosis. Arch Neurol 68, 1440–1446.

Ferreira JP, Overton KW, Wang CL (2013). Tuning gene expression with synthetic upstream open reading frames. Proc Natl Acad Sci USA 110, 11284–11289.

Freischmidt A, Wieland T, Richter B, Ruf W, Schaeffer V, Muller K, Marroquin N, Nordin F, Hubers A, Weydt P, *et al.* (2015). Haploinsufficiency of TBK1 causes familial ALS and fronto-temporal dementia. Nat Neurosci 18, 631–636.

Gijselinck I, Van Langenhove T, van der Zee J, Sleegers K, Philtjens S, Kleinberger G, Janssens J, Bettens K, Van Cauwenberghe C, Pereson S, *et al.* (2012). A C9orf72 promoter repeat expansion in a Flanders-Belgian cohort with disorders of the frontotemporal lobar degeneration-amyotrophic lateral sclerosis spectrum: a gene identification study. Lancet Neurol 11, 54–65.

Hara T, Takamura A, Kishi C, Iemura S, Natsume T, Guan JL, Mizushima N (2008). FIP200, a ULK-interacting protein, is required for autophagosome formation in mammalian cells. J Cell Biol 181, 497–510.

Hasumi H, Baba M, Hong SB, Hasumi Y, Huang Y, Yao M, Valera VA, Linehan WM, Schmidt LS (2008). Identification and characterization of a novel folliculin-interacting protein FNIP2. Gene 415, 60–67.

Jadot M, Boonen M, Thirion J, Wang N, Xing J, Zhao C, Tannous A, Qian M, Zheng H, Everett JK, *et al.* (2017). Accounting for protein subcellular localization: a compartmental map of the rat liver proteome. Mol Cell Proteomics 16, 194–212.

Jeffries TR, Dove SK, Michell RH, Parker PJ (2004). PtdIns-specific MPR pathway association of a novel WD40 repeat protein, WIPI49. Mol Biol Cell 15, 2652–2663.

Jung J, Nayak A, Schaeffer V, Starzetz T, Kirsch AK, Muller S, Dikic I, Mittelbronn M, Behrends C (2017). Multiplex image-based autophagy RNAi screening identifies SMCR8 as ULK1 kinase activity and gene expression regulator. Elife 6, e23063.

Leonetti MD, Sekine S, Kamiyama D, Weissman JS, Huang B (2016). A scalable strategy for high-throughput GFP tagging of endogenous human proteins. Proc Natl Acad Sci USA 113, E3501–E3508.

Levine TP, Daniels RD, Gatta AT, Wong LH, Hayes MJ (2013). The product of C9orf72, a gene strongly implicated in neurodegeneration, is structurally related to DENN Rab-GEFs. Bioinformatics 29, 499–503.

Maruyama H, Morino H, Ito H, Izumi Y, Kato H, Watanabe Y, Kinoshita Y, Kamada M, Nodera H, Suzuki H, *et al.* (2010). Mutations of optineurin in amyotrophic lateral sclerosis. Nature 465, 223–226.

Meng J, Ferguson SM (2018). GATOR1-dependent recruitment of FLCN-FNIP to lysosomes coordinates Rag GTPase heterodimer nucleotide status in response to amino acids. J Cell Biol, DOI: 10.1083/jcb.201712177.

Menon S, Dibble CC, Talbott G, Hoxhaj G, Valvezan AJ, Takahashi H, Cantley LC, Manning BD (2014). Spatial control of the TSC complex integrates insulin and nutrient regulation of mTORC1 at the lysosome. Cell 156, 771–785.

Nada S, Hondo A, Kasai A, Koike M, Saito K, Uchiyama Y, Okada M (2009). The novel lipid raft adaptor p18 controls endosome dynamics by anchoring the MEK-ERK pathway to late endosomes. EMBO J 28, 477–489.

O'Rourke JG, Bogdanik L, Yanez A, Lall D, Wolf AJ, Muhammad AK, Ho R, Carmona S, Vit JP, Zarrow J, *et al.* (2016). C9orf72 is required for proper macrophage and microglial function in mice. Science 351, 1324–1329.

Ostrowski PP, Fairn GD, Grinstein S, Johnson DE (2016). Cresyl violet: a superior fluorescent lysosomal marker. Traffic 17, 1313–1321.

Peli-Gulli MP, Sardu A, Panchaud N, Raucci S, De Virgilio C (2015). Amino acids stimulate TORC1 through Lst4-Lst7, a GTPase-activating protein complex for the Rag family GTPase Gtr2. Cell Rep 13, 1–7.

Petit CS, Roczniak-Ferguson A, Ferguson SM (2013). Recruitment of folliculin to lysosomes supports the amino acid-dependent activation of Rag GTPases. J Cell Biol 202, 1107–1122.

Ran FA, Hsu PD, Wright J, Agarwala V, Scott DA, Zhang F (2013). Genome engineering using the CRISPR-Cas9 system. Nat Protoc 8, 2281–2308.

Renton AE, Majounie E, Waite A, Simon-Sanchez J, Rollinson S, Gibbs JR, Schymick JC, Laaksovirta H, van Swieten JC, Myllykangas L, *et al.* (2011). A hexanucleotide repeat expansion in C9ORF72 is the cause of chromosome 9p21-linked ALS-FTD. Neuron 72, 257–268.

Richardson CD, Ray GJ, DeWitt MA, Curie GL, Corn JE (2016). Enhancing homology-directed genome editing by catalytically active and inactive CRISPR-Cas9 using asymmetric donor DNA. Nat Biotechnol 34, 339–344.

Roczniak-Ferguson A, Petit CS, Froehlich F, Qian S, Ky J, Angarola B, Walther TC, Ferguson SM (2012). The transcription factor TFEB links mTORC1 signaling to transcriptional control of lysosome homeostasis. Sci Signal 5, ra42.

Rodriguez-Paris JM, Nolta KV, Steck TL (1993). Characterization of lysosomes isolated from Dictyostelium discoideum by magnetic fractionation. J Biol Chem 268, 9110–9116.

Rubino E, Rainero I, Chio A, Rogaeva E, Galimberti D, Fenoglio P, Grinberg Y, Isaia G, Calvo A, Gentile S, *et al.* (2012). SQSTM1 mutations in frontotemporal lobar degeneration and amyotrophic lateral sclerosis. Neurology 79, 1556–1562.

Russell RC, Tian Y, Yuan H, Park HW, Chang YY, Kim J, Kim H, Neufeld TP, Dillin A, Guan KL (2013). ULK1 induces autophagy by phosphorylating Beclin-1 and activating VPS34 lipid kinase. Nat Cell Biol 15, 741–750.

Sancak Y, Bar-Peled L, Zoncu R, Markhard AL, Nada S, Sabatini DM (2010). Ragulator-Rag complex targets mTORC1 to the lysosomal surface and is necessary for its activation by amino acids. Cell 141, 290–303.

Saxton RA, Sabatini DM (2017). mTOR signaling in growth, metabolism, and disease. Cell 168, 960–976.

Sellier C, Campanari ML, Julie Corbier C, Gaucherot A, Kolb-Cheynel I, Oulad-Abdelghani M, Ruffenach F, Page A, Ciura S, Kabashi E, Charlet-Berguerand N (2016). Loss of C9ORF72 impairs autophagy and synergizes with polyQ Ataxin-2 to induce motor neuron dysfunction and cell death. EMBO J 35, 1276–1297.

Shi Y, Lin S, Staats KA, Li Y, Chang WH, Hung ST, Hendricks E, Linares GR, Wang Y, Son EY, *et al.* (2018). Haploinsufficiency leads to neurodegeneration in C9ORF72 ALS/FTD human induced motor neurons. Nat Med 24, 313–325.

Skibinski G, Parkinson NJ, Brown JM, Chakrabarti L, Lloyd SL, Hummerich H, Nielsen JE, Hodges JR, Spillantini MG, Thusgaard T, *et al.* (2005). Mutations in the endosomal ESCRTIII-complex subunit CHMP2B in frontotemporal dementia. Nat Genet 37, 806–808.

Stewart SA, Dykxhoorn DM, Palliser D, Mizuno H, Yu EY, An DS, Sabatini DM, Chen IS, Hahn WC, Sharp PA, *et al.* (2003). Lentivirus-delivered stable gene silencing by RNAi in primary cells. RNA 9, 493–501.

Stirnimann CU, Petsalaki E, Russell RB, Muller CW (2010). WD40 proteins propel cellular networks. Trends Biochem Sci 35, 565–574.

Sullivan PM, Zhou X, Robins AM, Paushter DH, Kim D, Smolka MB, Hu F (2016). The ALS/FTLD associated protein C9orf72 associates with SMCR8 and WDR41 to regulate the autophagy-lysosome pathway. Acta Neuropathol Commun 4, 51.

Takagi Y, Kobayashi T, Shiono M, Wang L, Piao X, Sun G, Zhang D, Abe M, Hagiwara Y, Takahashi K, Hino O (2008). Interaction of folliculin (Birt-Hogg-Dube gene product) with a novel Fnip1-like (FnipL/Fnip2) protein. Oncogene 27, 5339–5347.

Tharkeshwar AK, Trekker J, Vermeire W, Pauwels J, Sannerud R, Priestman DA, Te Vruchte D, Vints K, Baatsen P, Decuypere JP, *et al.* (2017). A novel approach to analyze lysosomal dysfunctions through subcellular proteomics and lipidomics: the case of NPC1 deficiency. Sci Rep 7, 41408.

Tsun ZY, Bar-Peled L, Chantranupong L, Zoncu R, Wang T, Kim C, Spooner E, Sabatini DM (2013). The folliculin tumor suppressor is a GAP for the RagC/D GTPases that signal amino acid levels to mTORC1. Mol Cell 52, 495–505.

Ugolino J, Ji YJ, Conchina K, Chu J, Nirujogi RS, Pandey A, Brady NR, Hamacher-Brady A, Wang J (2016). Loss of C9orf72 enhances autophagic activity via deregulated mTOR and TFEB signaling. PLoS Genet 12, e1006443.

van Blitterswijk M, Gendron TF, Baker MC, DeJesus-Hernandez M, Finch NA, Brown PH, Daughrity LM, Murray ME, Heckman MG, Jiang J, *et al.* (2015). Novel clinical associations with specific C9ORF72 transcripts in patients with repeat expansions in C9ORF72. Acta Neuropathol 130, 863–876.

Walker MW, Lloyd-Evans E (2015). A rapid method for the preparation of ultrapure, functional lysosomes using functionalized superparamagnetic iron oxide nanoparticles. Methods Cell Biol 126, 21–43.

Wall MA, Coleman DE, Lee E, Iniguez-Lluhi JA, Posner BA, Gilman AG, Sprang SR (1995). The structure of the G protein heterotrimer Gi alpha 1 beta 1 gamma 2. Cell 83, 1047–1058.

Wang T, Wei JJ, Sabatini DM, Lander ES (2014). Genetic screens in human cells using the CRISPR-Cas9 system. Science 343, 80–84.

Wang Y, Hu XJ, Zou XD, Wu XH, Ye ZQ, Wu YD (2015). WDSPdb: a database for WD40-repeat proteins. Nucleic Acids Res 43, D339–D344.

Webster CP, Smith EF, Bauer CS, Moller A, Hautbergue GM, Ferraiuolo L, Myszczynska MA, Higginbottom A, Walsh MJ, Whitworth AJ, *et al.* (2016). The C9orf72 protein interacts with Rab1a and the ULK1 complex to regulate initiation of autophagy. EMBO J 35, 1656–1676.

Wolfson RL, Sabatini DM (2017). The dawn of the age of amino acid sensors for the mTORC1 pathway. Cell Metab 26, 301–309.

Xiao S, MacNair L, McLean J, McGoldrick P, McKeever P, Soleimani S, Keith J, Zinman L, Rogaeva E, Robertson J (2016). C9orf72 isoforms in amyotrophic lateral sclerosis and frontotemporal lobar degeneration. Brain Res 1647, 43–49.

Xu J, McPherson PS (2017). Regulation of DENND3, the exchange factor for the small GTPase Rab12 through an intramolecular interaction. J Biol Chem 292, 7274–7282.

Yang M, Liang C, Swaminathan K, Herrlinger S, Lai F, Shiekhattar R, Chen JF (2016). A C9ORF72/SMCR8-containing complex regulates ULK1 and plays a dual role in autophagy. Sci Adv 2, e1601167.

Zhang D, Iyer LM, He F, Aravind L (2012). Discovery of novel DENN proteins: implications for the evolution of eukaryotic intracellular membrane structures and human disease. Front Genet 3, 283.